Thesis for The Degree of Licentiate of Engineering

Advanced Analog MMICs for mm-wave Communication and Remote Sensing in 0.15 μm mHEMT Technology

Marcus Gavell

Microwave Electronics Laboratory
Department of Microtechnology and Nanoscience (MC2)
Chalmers University of Technology
Göteborg, Sweden, 2013

Advanced Analog MMICs for mm-wave Communication and Remote Sensing in 0.15 μm mHEMT Technology

Marcus Gavell

Chalmers University of Technology
Department of Microtechnology and Nanoscience (MC2)
Microwave Electronics Laboratory
SE-412 96 Göteborg, Sweden
Phone: +46 (0) 31 772 1000

Technical report MC2-253
ISSN 1652-0769

Printed by Kompendiet
Göteborg, Sweden 2013

Abstract

Multi-Gigabit per second wireless communication and atmospheric remote sensing for weather forecasts are new applications in the mm-wave frequency spectra. The High Electron Mobility Transistor is an excellent technology for high frequency mm-wave applications. Its low noise and linear performance makes a 0.15 μm GaAs metamorphic HEMT technology the basis for three MMIC circuit designs at mm-wave frequencies.

The wireless data traffic has increased exponentially over the last years due to more network subscribers and their fast adaptation to use high data-rate mobile services. In order for the operators to evolve and accommodate higher data-rates at affordable prices, new microwave bands for point-to-point communication is a cost effective solution for increasing the backhaul capacity and deliver higher data rates to the network users. Two mm-wave mixers for wideband E-band communications, specially focusing on direct modulation and demodulation solutions have been designed, fabricated and characterized. Direct modulators requires added functions such as quadrature signals and LO-RF isolation to be compatible with e.g. QAM modulated signals. Complex high performance mixers with novel solutions have been designed to cope with cost, function and performance. Since cost is a driving factor, a novel differential branchline coupler has been introduced to reduce size while maintaining function and performance. The design rely on differential modes to accomplish this, something that is common in CMOS or BiCMOS due to the lossy substrate but not in GaAs. Utilizing the properties of common and differential modes, the LO-RF isolation has been further improved by the use of a mode selective filter. The design covers the whole E-band frequency span with measured 13 dBm OIP3, conversion loss of 11 dB, LO-RF isolation >30 dB and IF bandwidth of 5 GHz.

Remote mm and sub-mm wave sensing in Geostationary Earth Orbit has become an alternative solution for providing more accurate short term (nowcasting) weather predications. The advantage of being in geostationary orbit is the continuous coverage over a relatively large area. One of four frequency band of interest for this is 53 GHz, where a complete single chip MMIC receiver with integrated low noise amplifier, frequency multiplier and image reject mixer was designed, manufactured and measured. The Noise Figure (NF) of the receiver was measured to be 4.6 dB, with a total power consumption of 140 mW, conversion gain and image rejection measured to be 10 dB and >47 dB respectively. The NF is the lowest reported for a single chip receiver at 53 GHz.

Keywords: Mixers, Modulators, E-band, mm-wave, microwave, Point-To-Point, GaAs, HEMT, Geostationary, Receiver

Abbreviations and notations

Abbreviations

Explanations and comments on abbreviations used in the thesis.

2DEG	Two-dimensional electron gas
BER	Bit Error Rate
BEOL	Back End Of Line. The part of the process flow realated to fabrication of metal layers after the FEOL.
BPSK	Binary Phase Shift Keying
BiCMOS	Bipolar CMOS. Technology combining BJT or HBT and CMOS.
BJT	Bipolar Junction Transistor
BW	Band Width
CG	Conversion Gain
CL	Conversion Loss
CM	Common Mode
CMOS	Complementary Metal Oxide Semiconductor. Meaning p and n MOSFET devices in the same process.
CPW	Coplanar Waveguide
DBC	Differential Branchline Coupler
DM	Differential Mode
DUT	Device Under Test
FCC	Federal Communications Commission
FET	Field Effect Transistor
FOM	Figure of Merits
GAS	Geostationary Atmospheric Sounder
GbE	Gigabit Ethernet
GEO	Geostationary Earth Orbit

GSG	Ground-Signal-Ground
GSM	Global System for Mobile Communications
HBT	Heterojunction Bipolar Transistor
HD	High Definition
HEMT	High Electron Mobility Transistor
HM	Harmonic Mixer
IF	Intermediate Frequency Here used to mean frequencies below 10 GHz.
IIP3	Input Third order intercept point
IM	Intermodulation
IP1dB	Input referred 1 dB compression point
IP3	Third order intercept point
IQ	In phase and Quadrature
IRM	Image Reject Mixer
IRR	Image Rejection Ratio
LEO	Low Earth Orbit
LNA	Low Noise Amplifier
LO	Local Oscillator
LSB	Lower Side Band
mHEMT	metamorphic High Electron Mobility Transistor
MMIC	Monolithic Microwave Integrated Circuit
NF	Noise Figure
OIP3	Output Third order intercept point
P1dB	1 dB compression point
P2P	Point-To-Point
pHEMT	pseudomorphic High Electron Mobility Transistor
QAM	Quadrature Amplitude Modulation
RBS	Radio Base Station
RF	Radio Frequency Here used to mean frequencies above 10 GHz.
USB	Upper Side Band

Notations

f_t	Transit frequency
f_{max}	Maximum oscillation frequency
Gbps	Gigabit per second
Mbps	Megabit per second
V_{gs}	Gate-Source Voltage
R_{ds}	Channel Resistance
C_{gd}	Gate-drain capacitance
P_{LO}	LO power
P_{IF}	IF power
P_{RF}	RF power
f_{LO}	LO frequency
f_{IF}	IF frequency
f_{RF}	RF frequency
q	Electron charge (Coulomb)

List of Publications

Appended Publications

This thesis is based on work contained in the following papers:

[A] M. Gavell, M. Ferndahl, S. E. Gunnarsson, M. Abbasi, and H. Zirath "An Image Reject Mixer for High-Speed E-band (71-76, 81-86 GHz) Wireless Communication" presented at *IEEE Compound Semiconductor Integrated Circuits Symposium (CSICS) Conference*, Greensboro, NC, USA, 2009.

[B] M. Gavell, H. Zirath, M. Ferndahl and S. E. Gunnarsson, "A linear 70-95 GHz differential IQ modulator for E-band Wireless Communication," presented at *IEEE International Microwave Symposium (IMS) Conference*, Anaheim, CA, USA, 2010.

[C] M. Gavell, M. Ferndahl, S. E. Gunnarsson, H. Zirath, "A 53 GHz single chip Receiver for Geostationary Atmospheric Measurements," presented at *IEEE Compound Semiconductor Integrated Circuits Symposium (CSICS) Conference*, Kailua Kona, HI, USA, 2011.

Other Publications

The following paper has been published but is not included in the thesis. The content partially overlaps with the appended papers or is out of the scope of this thesis.

[a] M. Gavell, M. Ferndahl, H. Zirath, M. Urteaga and R. Pierson "A fundamental upconverting Gilbert mixer for 100 GHz wireless applications," presented at *IEEE Compound Semiconductor Integrated Circuits Symposium (CSICS) Conference*, Monterey, CA, USA, 2010.

[b] S.E. Gunnarsson, M. Gavell, D. Kuylenstierna and H. Zirath "60 GHz MMIC double balanced Gilbert mixer in mHEMT technology with integrated RF, LO and IF baluns" *ELECTRONICS LETTERS 23rd November 2006 Vol. 42 No. 24*

[c] W. Keusgen, A. Kortke, L. Koschel, M. Peter, R. Weiler, H. Zirath, M. Gavell and Z. He "An NLOS-Capable 60 GHz MIMO Demonstrator: System Concept & Performance" presented at *IEEE New Circuits and Systems Conference (NEWCAS)*, Bordeaux, France, 2011

Contents

Chapter 1

Introduction

1.1 Motivation

Applications in high speed communications and remote sensing have found their way into mm-wave frequencies. The atmospheric conditions and licensing part of the frequency spectrum have attracted these two different applications to this frequency range. The development of semiconductor technologies have pushed Monolithic Microwave Integrated Circuit (MMIC) circuit designs to and beyond mm-waves [1]. The High Electron Mobility Transistor (HEMT) is one of possible semiconductor technologies to use in this frequency range and it shows excellent performance for MMIC designs. Low noise and linear performance made this technology the choice for the work presented in this thesis.

The technology development in the field of electronics has since the dawn of the integrated circuit changed our way of living. Wireless communication and flow of information have probably contributed to the biggest change. Mobile voice service is already considered a necessity by most, and mobile data, video, and TV services are fast becoming an essential part of everybody's lives. In 2009, for the first time in history, the data traffic was reported to be higher than voice traffic and the trend is continuous [2]. The origin of the standardized wireless infrastructure for mobile phones, Global System for Mobile Communications (GSM), is a great achievement over the last decades and has paved the way for an incredible research and development in the area of electronics for wireless communication. GSM was the first digital cellular system (2G) replacing the analog cellular network (1G). The 2G system was developed over time to handle data traffic and today, the forth generation standard (4G LTE Advanced) is in use. The expected wireless traffic contributed over the mobile networks is plotted in Figure 1.1 for the coming 5 years. The number of mobile subscribers is growing rapidly and the demand for bandwidth due to data and video is increasing fast. Today, microwave backhauls are reported to be the bottleneck in the wireless networks [3]. To allow mobile broadband, data access, and video services to effectively grow and follow consumer usage trends, the capacity of the microwave backhaul must allow higher data rates and lower the cost per bit [3].

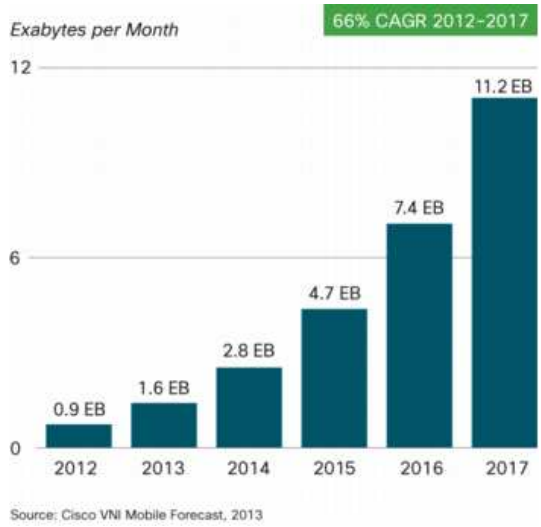

Figure 1.1: Cisco Visual Networking Index for the expected data traffic in the mobile networks [3].

1.2 Atmospheric windows

The atmospheric conditions are important to consider when choosing the frequency for the application. Up to around 50 GHz the atmospheric conditions are similar and the Point-To-Point (P2P) radios in the microwave bands have similar conditions and are regulated equally around the world [4]. Above 50 GHz the propagation condition changes and with this also the regulations [5] and applications. In Figure 1.2, the atmospheric propagation loss is showed in a logarithmic scale from 1 up to 300 GHz. Absorption peaks are found at 23, 60, 119 and 183 GHz and on the contrary, minimum attenuation occurs at 80, 140 and 220 GHz, referred to as atmospheric windows. Both absorption and minima bands are interesting from high speed communications point of view, but with different applications in mind. The absorption bands have shown interest in radars, remote sensing and secure and short range communications while the minima bands mainly show interest for P2P communication. High attenuation ensure secure and short range transmissions, it can for instance transfer High Definition (HD) video a few meters at home. Remote sensing for meteorological and climate observation using Geostationary Earth Orbit (GEO) satellites are consider for future satellites and the prioritized frequency bands are close to the absorption peaks [6]. P2P communication on the other hand wants to cover long distances, therefore low attenuation is required.

1.3 Thesis contribution

The evolution of P2P microwave links has since the start developed higher modulation formats to cope with higher data rates and spectral efficiency. High speed communications in the mm-wave frequency spectra require advanced and high performing circuits to cope with high order modulation and

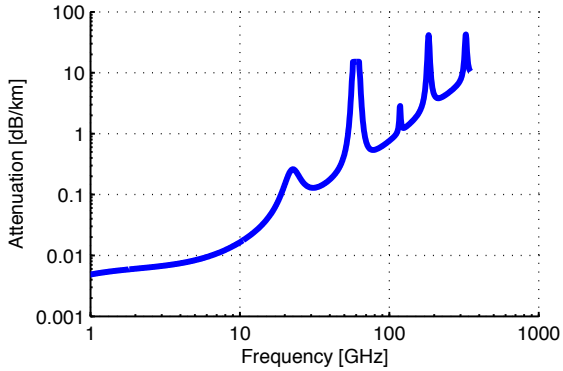

Figure 1.2: Atmospheric attenuation in the earth's atmosphere for vapor concentration of $10\,\mathrm{g/m^3}$ [7].

medium long distances. Two quadrature mixers for E-band communications have been designed, fabricated and characterized for their Radio Frequency (RF) performances. New circuit concepts have been evaluated for minimizing size and maintaining or improving performance for high speed communications in the E-band. In [A], a direct down-conversion quadrature mixer is presented and in [B] a balanced quadrature mixer with a novel topology to suppress Local Oscillator (LO) on the RF port is presented. The novelty design benefits from using the differential and common mode properties, such that balance and performance of the circuit is improved. Economical aspects are also positive, since the two signal mode design makes the circuit size smaller in comparison to traditional single mode circuits. The results show, low Conversion Loss (CL), high linearity and high Image Rejection Ratio (IRR) for both concepts.

A low noise 53 GHz single chip receiver for atmospheric remote sensing is presented in [C]. The single chip receiver consists of three integrated functions on chip; a Low Noise Amplifier (LNA), a $\times 4$ multiplier and an Image Reject Mixer (IRM) to ease mounting of the 136 elements of 53 GHz receivers in the proposed weather satellite [6]. The RF performance of a single chip is also expected to be better than discrete solution. Of the reported single chip receivers at 53 GHz in the open literature, this reports the lowest Noise Figure (NF) and highest IRR.

1.4 Thesis outline

The thesis focuses on the design of MMIC mixers for high speed P2P communications in the mm-wave frequency bands. Chapter 2, section 2.2 briefly describes the mixing fundamentals for the resistive mixer and the HEMT technology that has been used in all circuit designs [A-C]. The same section touches on different mixer topologies and compare topologies and my work with others. In section 2.2.3, different mixer error mechanisms that relates to increased Bit Error Rate (BER) are isolated and discussed. With some theory, technology background and system considerations in mind, two circuit designs from [A,

B] are presented in sections 2.4 and 2.3. In chapter 3, the design and characterization of a 53 GHz receiver for atmospheric remote sensing is presented [C]. The thesis is concluded in chapter 4 with some final words about future work.

Chapter 2

Mixers for E-band communications

The mixer is an essential component for communication systems. Its function is to convert an input signal to another frequency while maintaining information about the amplitude and phase. This is the reason why wireless communication is possible at any frequency. By multiplying the input signal with the LO, the frequency conversion is achieved. In Figure 2.1, a block diagram of a homodyne receiver and transmitter front-end for a wireless communication link shows the mixer as the central part of such system. The mixing function can be realized both from nonlinear and time-varying topologies based on semiconductor technologies. Mm-wave mixers were for a long time based on rudimentary diode mixers but recent years' process development has allowed MMIC to be designed well into the sub-mm wave and even sub-THz regions [1]. This has lead the way to the most complex and state of the art performing mm-wave mixers to be based on advanced transistor technology. Technologies based on HEMT, Complementary Metal Oxide Semiconductor (CMOS), Bipolar CMOS (BiCMOS) and Heterojunction Bipolar Transistor (HBT) based on SiGe and InP are possible processes to use.

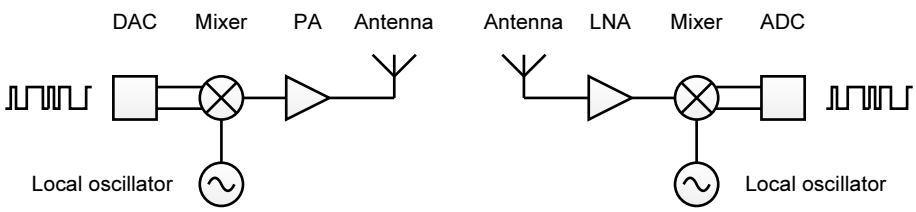

Figure 2.1: Wireless link for P2P communication.

This chapter provides a summary on mixer topologies and an introduction to semiconductor technology, focusing on HEMT which is the technology used in [A-C]. The curious reader with interest in other semiconductor technologies is kindly referred to [8]. The chapter also includes a short discussion about mixer Figure Of Merits (FOM), their relevance and the effect from a system's perspective. A survey of mm-wave mixers are shown and the results

are compared with my work on this topic. Finally, two original mixer designs for E-band communications will be described and presented.

2.1 Microwave backhaul

In the wired world, multi gigabit data transmission has been commercially available for a long time. Standard protocols such as Gigabit Ethernet (GbE) protocols are sold in millions of commercial devices. Even faster protocols in fiber optic networks exists, where 10-GbE, 40-GbE[1] and 100-GbE[1] are standards for the service of the backbone wired network structures. Using fibers has many positive aspects, they are secure, reliable, provide excellent service and speed. However, deploying fibers struggles with installation time, maintenance, cause disruption and cost which in the end affects the users.

For many years now, microwave bands between 6 and 40 GHz have been used for P2P backhauling but the data transmission speed has been far behind fiber optics. The reason for this is simple, the lack of bandwidth. At the microwave bands, the available channel bandwidth is up to 56 MHz, whereas for fiber several GHz. At the time when the microwave bands were defined, transferring voice was the main purpose and channel bandwidth was relatively narrow but for transferring data with high speed, wide bandwidth or many symbols per Hz is necessary. The narrow bands use high order modulation to increase the spectral efficiency and offer more throughput.

The start for licensed wideband P2P communications came in 2003 when the Federal Communications Commission (FCC) regulated the E-band for P2P communication. In Figure 2.2, the microwave bands for P2P communication are illustrated together with the wide band 60 GHz and E-band (71-76, 81-86 and 92-95 GHz). The difference in terms of bandwidth between the established microwave bands and the newer are obvious. Even though the E-band is specified to three separate bands, the former two are usually referred to as the E-band, and will be so throughout the thesis. Here labeled E1 (70), E2 (80) and E3 (90), shown in Figure 2.2.

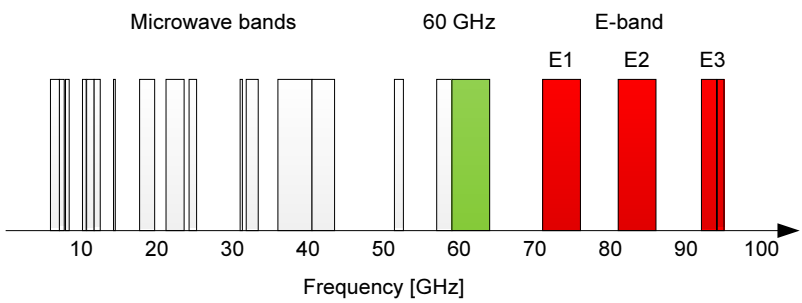

Figure 2.2: Illustration of bandwidth in licensed P2P communication links.

Utilizing the available bandwidth at mm-wave, some high speed wireless transmission $\geq$10 Gbps has been reported at 70/80, 120 and 220 GHz in [9], [10] and [11] respectively. The high frequency demonstrations use simple modulation and high bandwidth to achieve such high data rate transmission. This

[1] IEEE 802.3ba

is completely the opposite to microwave band radios, where bandwidth is a limiting factor and throughput is difficult to increase further. Already today, many bits per symbol are used in the microwave band radios.

A typical backhaul network infrastructure together with RBSs (Radio Base Station) and fiber Ethernet network is shown in Figure 2.3. As can be seen in this illustration, the microwave backhaul is an essential part of the network infrastructure but the maximum data-rate is limited by the P2P links to 750 Mbps.

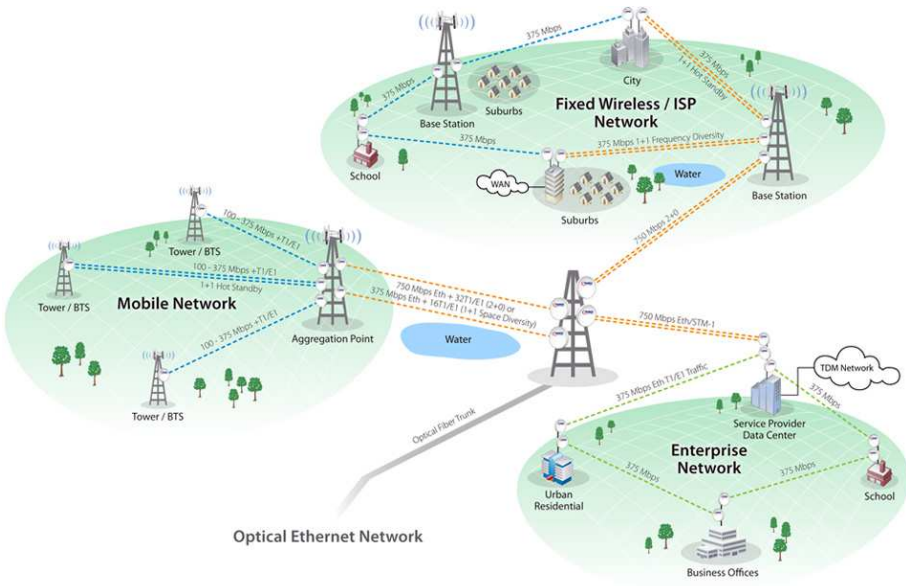

Figure 2.3: Backhaul network infrastructure.
Source: ©TrangoSystem 2013

2.2 Mixer fundamentals

2.2.1 Mixer Topologies

There are numerous mixer topologies and technologies to choose from to realize a mixer. A short description and comparison of the most common mixer topologies are presented in Table 2.1 and along the text. FOM for relevant mixers in the same frequency range and function have been included in the comparison.

The Gilbert cell

The Gilbert cell was introduced by Barrie Gilbert as a precision multiplier but is widely used as a mixer in modern communication systems [12]. The advantages with the Gilbert cell is that it provides high Conversion Gain (CG), high frequency of operation and high port-to-port isolation. Its principle of operation is technology independent and can be realized in Bipolar Junction Transistor (BJT) or Field Effect Transistor (FET) technology. The main drawback with the standard form of the

Gilbert cell is its limited linearity and NF. Due to it's popularity, several techniques have been proposed to overcome these issues. In [13], a charge injection method for CMOS technology was suggested to improve those numbers. Third order intermodulation cancellation or feedforward techniques are other techniques that improve linearity [14]. Unfortunately, these solutions tend to be frequency or bias sensitive. The iconic Barrie Gilbert published in 1997 "The MICROMIXER" [15], a version of the classical Gilbert cell replacing the problematic transconductance stage with a bi-symmetrical class-AB input stage to improve linearity. The design of the input stage limits the frequency range but has been reported as high as 77 GHz [16].

Resistive FET mixer

The resistive FET mixer, first proposed by S. Maas in 1987 [17], is widely used due to its high linearity, simple implementation and low DC consumption. In this topology, the transistor is working in the linear region, below the knee as illustrated in Figure 2.4a. The applied LO voltage at the gate controls the channel resistance R_{ds} as a time varying resistance to perform mixing. The control action is illustrated in Figure 2.4b. Since the resistance is weakly non-linear below the knee, the Intermodulation (IM) products are low even for moderate LO power.

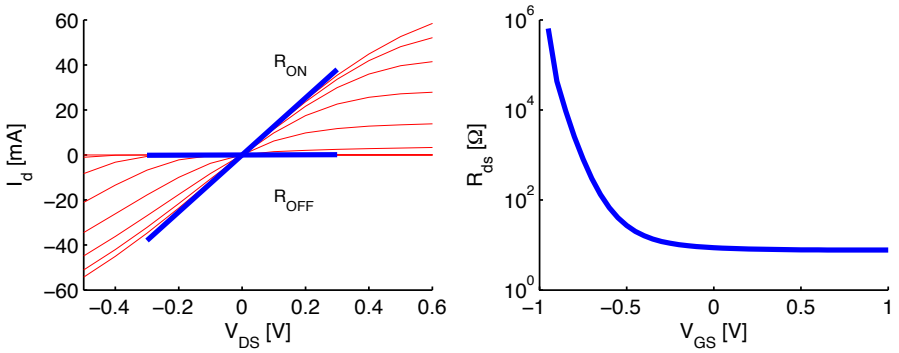

(a) Principle of operation (b) Channel resistance dependence on V_{gs}

Diode mixer

The diode is a strongly non-linear element and diode mixers make use the exponential transfer function $I_C \sim exp(V_C)$ of the diode to perform mixing products. The mixer design doesn't need to be strongly non-linear if designed properly though. The diode is preferably driven by a high-powered LO source to assure effective switching between ON and OFF states to direct the RF signal and generate mixing products. In contrast to FET mixers, there is no independent control of the channel resistance which makes the diode mixers less linear for a given LO power. Moreover, due to rectification of the LO through the diode, this introduces noise which is disadvantageous [18].

Comparing mixers is sometimes ambiguous and difficult to interpret due to their different functions, up- or down-conversion characterization, active

output buffer amplifiers etc. Luckily, common parameters for mixers exists and are included in the comparison in Table 2.1.

In terms of linearity (1 dB compression point (P1dB) and Third order intercept point (IP3)), the resistive mixers report among the highest results, including my work. The Output IP3 (OIP3) in [B] shows 13 dBm and Output P1dB (OP1dB) during 2-tone measurement of 0 dBm. The OIP3 is far better than [19] and [16] but lower OP1dB than [16] and [20]. In [21], a buffer amplifier is included which disqualifies it in the comparison.

Active mixers such as the Gilbert cell, has the characteristic of achieving positive CG, but this feature does not necessarily need to be advantageous. For instance, increased CG will reduce the Input IP3 (IIP3) of the mixer, which might be disadvantageous. Nevertheless, all active mixers show higher CG than the passive mixers.

NF is only reported in two of the references, the micromixer and a diode mixer [16] and [22] respectively. In this duel, the diode mixer is a clear winner, the others can only be speculated or referred to theory. In theory though, the FET technology has an advantage over BJT and HBT technology in terms of noise. HBTs and BJTs introduce shot-noise since they always need base current I_b to operate, something FETs simply are free from. Therefore, the NF of a FET is normally lower to that of a BJT. In the case of the resistive mixer, the generated noise is purely thermal, therefore the NF is comparable to the CL. FETs also have a slight edge in added noise compared to diodes due to the rectification of LO current.

The topologies seem not to have any large influence on the function. For the reported IRR and LO-RF isolation, most show similar number which indicates that the topology doesn't affect the function.

Ref	Freq [GHz]	CL	IRR	LO-RF	P1dB	OIP3	NF	Size [mm^2]	Topology	Technology
[23]	55-66	11± 0.5	> 24	> 25	-5.6	n/a	n/a	2.875	Up-conversion Double Balanced Resistive Mixer	0.15 μm HEMT
[21]	77	n/a	> 28	> 23	2.5	n/a	n/a	1.35	Up-conversion Gilbert cell	0.35 μm SiGe HBT
[24]	50-110	13± 0.5	> 21	> 23	n/a	n/a	n/a	4	Reflection based phase shifter	1 μm GaAs HBT
[19]	57-66	14± 1.5	> 19	> 35	-13	4	n/a	2.25	Up-conversion Single Balanced resistive mixer	0.25 μm GaAs pHEMT
[16]	77	−13.4	n/a	> 34	1.4	8	18.4	0.275	Down-conversion Micromixer	0.25 μm SiGe BiC-MOS
[11]	75-95	12± 1	n/a	n/a	-11	n/a	n/a	2.81	Down-conversion Single Balanced resistive mixer	50 nm GaAs mHEMT
[25]	25-75	3 ± 2	n/a	n/a	-4	n/a	n/a	0.3	Down-conversion Gilbert cell	90 nm CMOS
[22]	94	11	16	n/a	n/a	n/a	12	2.5	Down-conversion Schottky diode	0.1 μm GaAs pHEMT
[20]	94	3	n/a	33	5	n/a	n/a	3.8	Down-conversion Single Balanced gate mixer	0.07 μm GaAs mHEMT
[B]	70-95	11± 0.5	> 20	> 30	0	13	n/a	3.75	Up-conversion Single Balanced resistive mixer	0.15 μm GaAs mHEMT
[A]	71-86	9 ± 0.5	> 15	n/a	-5	n/a	n/a	3	Down-conversion Resistive mixer	0.15 μm GaAs mHEMT

Table 2.1: Comparison of mm-wave mixers

2.2.2 Technology (GaAs mHEMT)

The circuits in papers A-C were designed in 0.15 μm GaAs metamorphic HEMT (mHEMT) technology, for good reasons. It's a mature and stable

technology and provides overall good high frequency performance. The main drawback with GaAs HEMT technology is the chip area, mainly due to the less advanced Back End of Line (BEOL) but to some extent to the higher current density in HBTs and CMOS which makes the physical size of those transistors smaller. All Gilbert cell based mixers in SiGe HBT, BiCMOS or CMOS are considerably smaller in size, around 1:10 of the circuits included in the comparison in Table 2.1.

A HEMT is a FET based on a heterostructure that confines the electrons in a high mobility channel [26]. The principle idea is to physically separate the donors from the electrons to avoid ionized impurity scattering between them. This increases the mobility of the electrons, transit time across the channel decreases, therefore f_t increases and thus the maximum frequency of operation is higher [8].

A typical schematic and conduction band profile for a GaAs HEMT are illustrated in Figure 2.5. The lower bandgap material in the channel (usually InGaAs) and the higher bandgap barrier material form a heterojunction that imposes an energy barrier that confines electrons in the channel forming a two dimensional electron gas (2DEG). Free carriers are introduced by adding a thin highly doped δ-layer, separated a certain distance towards the undoped channel (spacer) and a barrier towards the Schottky contact. The conduction band energy under the gate is shown in cross section A-A' and how the electrons are confined in the channel. The channel current is controlled by the Schottky contact on top of the barrier which changes the Fermi level in the semiconductor with $-qV_{gs}$ when increasing or decreasing the gate voltage. To the left in Figure 2.5, electrons are confined in the 2DEG and to the right, the channel is depleted.

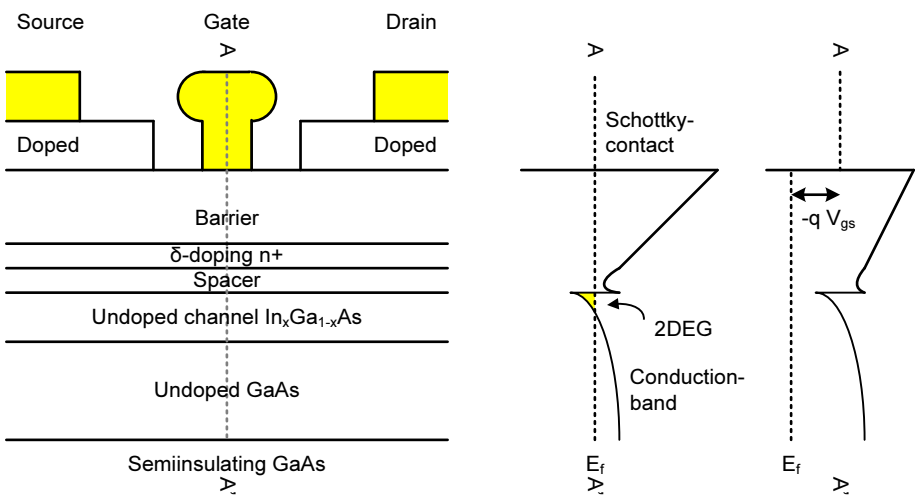

Figure 2.5: Cross section and conduction band profile of a HEMT.

2.2.3 FOM

The common FOM for a quadrature mixer are linearity, CG, NF, quadrature balance and port-to-port isolation. These parameters are all relevant for any

mixer but depending on the application, some are more important than others. In digital communications, low BER, high dynamic range and high throughput are characteristics for a wireless link's performance. The maximum throughput of a link is the available RF bandwidth × number of bits per symbols and the upper bound for symbol efficiency (Nyquist rate, bits per Hz) is given by $N = \log_2(M)$. M is the number of symbols and N then the symbol efficiency in bits per symbol. Quadrature Amplitude Modulation (QAM) is one of the most common and spectral efficient modulation formats that is flexible to these characteristics of a receiver. These characteristics include accuracy of the amplitude, phase, and frequency of each baseband signal. For simple modulation schemes such as 4-QAM or Binary Phase Shift Keying (BPSK), relatively inaccurate baseband signals are tolerable but the symbol efficiency is lower. However, for higher order modulation schemes such as 64-QAM and 256-QAM, baseband accuracy is essential. For these modulation schemes, small errors of DC offset, phase noise, quadrature skew, or IQ gain imbalance can make the transitions of the RF signal too difficult to distinguish.

As an example of deteriorations to increased BER, six impairments on a 64-QAM signal are illustrated in Figure 2.6. They include added noise, quadrature skew, In phase and Quadrature (IQ) gain error, phase noise and DC offset from Figure 2.6a-2.6f. The different errors are added to the ideal expression for the output waveform in equation 2.1 and given in equations 2.2-2.5. The output waveform of an ideal modulator $s(t)$ is expressed in equation 2.1, where I and Q are the two inputs and ω_0 is the carrier frequency.

$$s(t) = \mathbb{R}\left\{\left[I(t) + jQ(t)\right] e^{j\omega_0 t}\right\} = I(t)\cos(\omega_0 t) - Q(t)\sin(\omega_0 t) \tag{2.1}$$

Figure 2.6a illustrates added thermal noise (Johnson noise) which also determines the lowest possible received power level and the low limiting factor in the dynamic range of a receiver. Added noise is illustrated in Figure 2.6a and is expressed in equation 2.2.

$$s(t) = \mathbb{R}\left\{\left[I(t) + jQ(t) + w_{noise}\right] e^{j\omega_0 t}\right\}, w_{noise} \in \mathbb{C} \tag{2.2}$$

Phase noise appears as illustrated in Figure 2.6b. This noise is contributed from the carrier signal rather than from the mixer. Equation 2.3 shows that the output expression and the phase noise ϕ_{noise} belongs to the carrier expression $e^{j\omega_0 t + j\phi_{noise}}$ and not from the input data.

$$s(t) = \mathbb{R}\left\{\left[I(t) + jQ(t)\right] e^{j\omega_0 t + j\phi_{noise}}\right\} \tag{2.3}$$

The quadrature balance is a combined measure of the gain and phase error, shown in Figure 2.6c and 2.6d. The combined expression for gain and phase error is shown in equation 2.4.

$$s(t) = \mathbb{R}\left\{\left[I(t) V_I e^{j\phi_I} + jQ(t) V_Q e^{j\phi_Q}\right] e^{j\omega_0 t}\right\} \tag{2.4}$$

The upper limiting factor in the dynamic range appears as compression, shown in Figure 2.6e. The linearity is either measured as P1dB or IM products.

LO leakage from the transmitter will appear as a DC offset on the two received I and Q baseband channels. As in any mixing, the outcome of two

identical signals will be $f_{LO} \pm f_{LO}$, thus a DC level plus a $2f_{LO}$ component. The $2f_{LO}$ product can simply be filtered but the DC component might be problematic unless AC coupled pattern is used. Equal DC offset on the two channels is illustrated in Figure 2.6f and equation 2.5. A large LO leakage on the transmitter will be amplified in the band and affect the performance of the transmitter, leading to lower output power and IP3 of the converted signal.

$$s(t) = \mathbb{R}\left\{\left[I(t) + I_{DC} + j\left(Q(t) + Q_{DC}\right)\right] e^{j\omega_0 t}\right\} \tag{2.5}$$

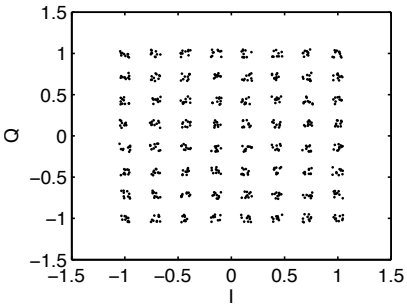

(a) Johnson noise, Temperature noise

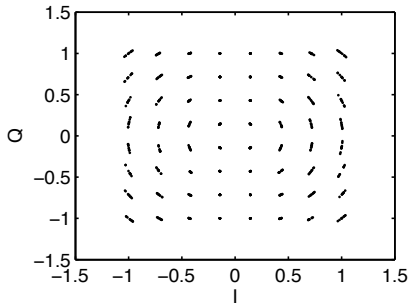

(b) Phase noise

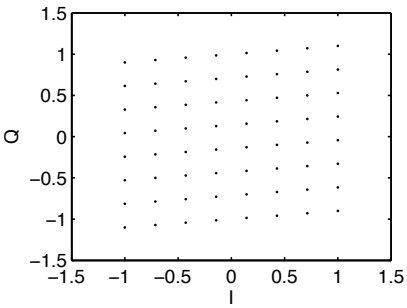

(c) IQ phase noise

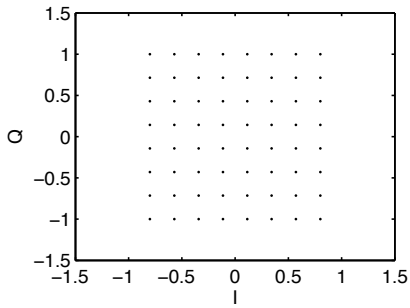

(d) IQ gain error

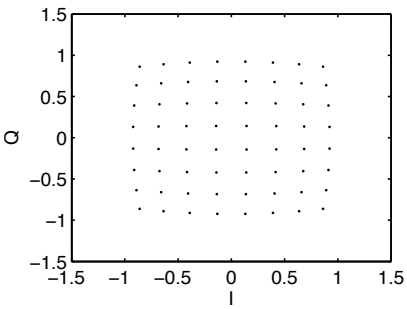

(e) IF compression

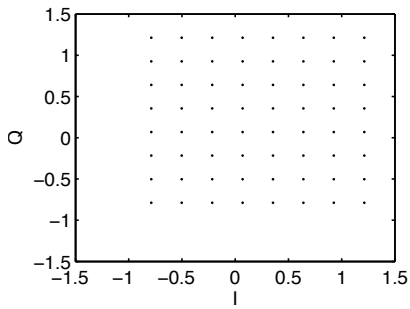

(f) DC offset

Figure 2.6: Typical impairments on a 64 QAM constellation

2.3 Single balanced IQ modulator

The target area and application for the circuit presented in this section is to be used as a direct modulator in front-end transmitters for wideband wireless communication at all three E-bands (E1, E2 and E3). Using a direct modulator reduces the number of components in the front-end but requires more complex design, both in terms of RF performance and function. A direct modulator need high requirements on the LO residual as well as linearity and IQ phase and amplitude balance as described in section 2.2.3. Apart from the RF requirements, to work throughout the complete E-band frequency span, the circuit must cover 71-95 GHz, a relative bandwidth of 29% which is a challenging task. The implementation and measurements of the circuit were reported in paper B.

2.3.1 Design

In order to design a linear mixer with quadrature input and inherent LO-RF isolation over a wide bandwidth, many observations and design considerations were made. In the following paragraphs, prospects and consequences of different solutions are discussed.

LO to RF port isolation is one of many requirements that are important in order to design a direct conversion mixer with quadrature input. In [27], a structure with inductive feedback between the LO and RF ports (here the gate and drain terminal), tried to isolate the ports from each other based on parallel resonance with C_{gd} and the external inductance. This solution is though more sensitive to process variations, it's frequency dependent and less linear than a balanced structure. To achieve high LO to RF isolation over a wide bandwidth, a balanced structure was chosen to isolate the LO and RF ports from each other. A balanced structure does also give higher linearity but require higher LO power and make the chip size larger. In principle, a combination of two circuits from paper A, would add LO-RF isolation functionality to the chip but the chip size would in the best case be $2 \times 2 \times 1.5\,\mathrm{mm}^2$, a disadvantage in terms of costs. Instead, the idea of using differential mode (DM) in combination with quadrature signals internally on the chip via a Differential Branchline Coupler (DBC) resulted in a considerably smaller chip. In total, the chip size is reduced to $2.5 \times 1.5\,\mathrm{mm}^2$. Figures 2.7 and 2.8 show the layout and the schematic of the design respectively. A solution with a DBC integrated on chip was published in paper [21], a SiGe technology where circuit designers often use differential signals or CoPlanar Waveguide (CPW) to avoid propagating signals in the lossy substrate. The DBC is presented in more detail in section 2.3.2. To further improve the LO-RF isolation, and taking advantage of the differential and common-modes, a Common-Mode (CM) filter is implemented. This feature is described in detail in section 2.3.3.

The resistive mixer topology was chosen as a basis of the design, and the main reason for the choice comes from a linearity perspective. The transistor size in the design was chosen to be $2 \times 50\,\mu m$. A large device has lower R_{ON} resistance and will thus give lower CL and higher linearity but will require more LO power due to the increased intrinsic capacitances of the transistor. The transistor model used in the design was a EEHEMT [28] provided from

WIN semiconductors.

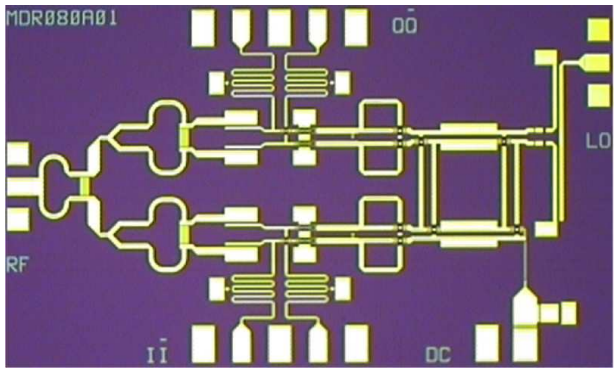

Figure 2.7: Photo of the single balanced IQ mixer

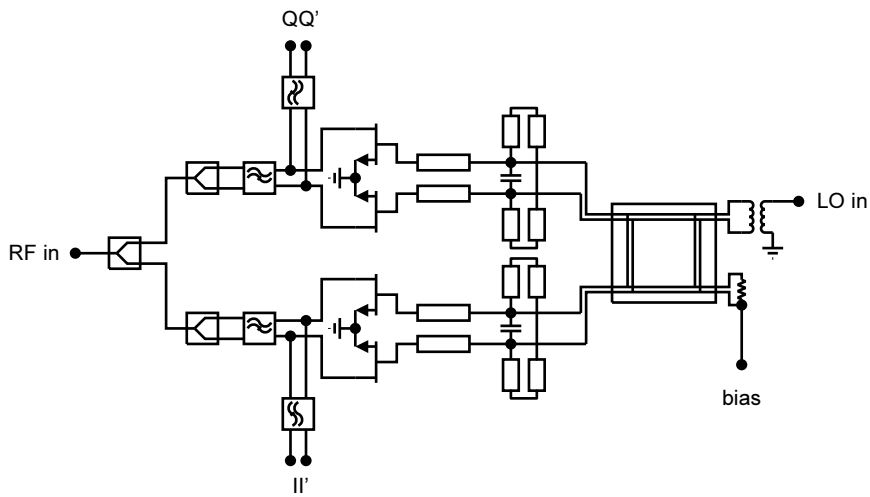

Figure 2.8: Schematic of the single balanced IQ mixer

2.3.2 Differential Branchline Coupler

A balanced quadrature design require that either the LO or RF must be converted into phase states of 0°, 90°, 180° and 270° with equal amplitude. The 0° and 90° split are for the quadrature signals and the remaining 180° and 270° to make the quadrature signals differential. The DBC is designed to acquire differential quadrature signals from a differential source, such that the outcome with be phase shifted 0°, 90°, 180° and 270° degrees. The layout and schematic are shown in Figure 2.9 and 2.10 respectively. The lengths, DM characteristic impedances of the lines and the termination are marked in Figure 2.10. Because the differential performance is the most important mode for this design, the termination is purely differential, i.e. 100 Ω between the lines.

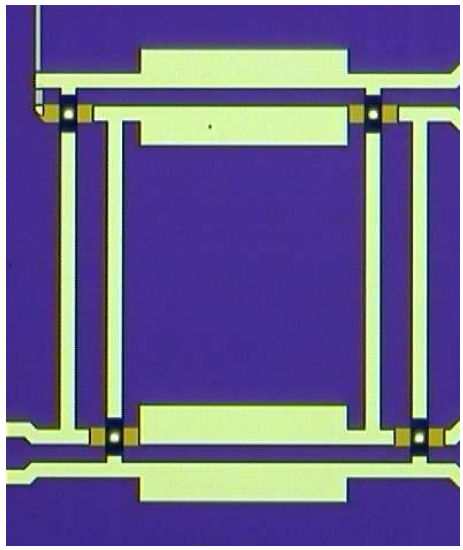

Figure 2.9: Layout of the DBC

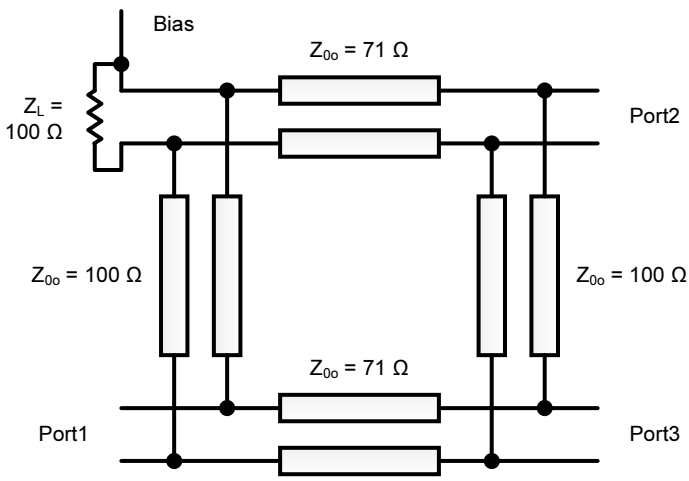

Figure 2.10: Schematic of the DBC

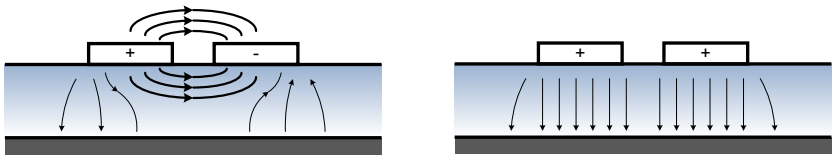

(a) Differential mode (b) Common mode

Figure 2.11: Illustration of the two modes propagating along a coupled line.

The principle of the DBC is exactly the same as the branch-guide or branchline design [29], the only difference is the propagating mode. It uses four sections of quarter wavelength transmission lines with odd mode characteristic impedances of $Z_{0o} = 71\ \Omega$ and $Z_{0o} = 100\ \Omega$, the same as any branchline design in a 100 Ω environment. In principle, two microstrip branchline couplers are put on top of each other such that two modes can propagate along the transmission lines, the CM and the DM. The two modes are illustrated in Figure 2.11, in Figure 2.11a the wanted DM and in Figure 2.11b, the unwanted CM.

Simulation results of the differential response from the DBC are shown in Figure 2.12. Phase and amplitude balance between port 2 and 3 and return loss are shown in Figure 2.12a, 2.12b and 2.12c respectively. The results show better than 1 dB amplitude error, 5° degree phase error and 10 dB port matching over a frequency span from 65 to 92 GHz. CM generation in Figure 2.12d is important to keep low, such that the LO and RF ports are isolated from each other. This FOM is better than 25 dB for both ports in the same frequency span as mentioned above. To present the performance of the DBC in matrix form with respect to CM and DM, the most intuitive way is from a mixed mode matrix [30]. Equation 2.6 shows the structure of a 3-port mixed mode S-parameter matrix with DM and CM excitation on the three ports and thus the DM-DM, DM-CM, CM-DM and CM-CM response. Here, the DM-DM response is the most important parameter but the DM-CM transformation is also of interest because of the decrease in LO-RF isolation and differential balance.

$$S = \begin{bmatrix} S_{DD} & S_{DC} \\ S_{CD} & S_{CC} \end{bmatrix} = \left[\begin{array}{ccc|ccc} S_{1D1D} & S_{1D2D} & S_{1D3D} & S_{1D1C} & S_{1D2C} & S_{1D3C} \\ S_{2D1D} & S_{2D2D} & S_{2D3D} & S_{2D1C} & S_{2D2C} & S_{2D3C} \\ S_{3D1D} & S_{3D2D} & S_{3D3D} & S_{3D1C} & S_{3D2C} & S_{3D3C} \\ \hline S_{1C1D} & S_{1C2D} & S_{1C3D} & S_{1C1C} & S_{1C2C} & S_{1C3C} \\ S_{2C1D} & S_{2C2D} & S_{2C3D} & S_{2C1C} & S_{2C2C} & S_{2C3C} \\ S_{3C1D} & S_{3C2D} & S_{3C3D} & S_{3C1C} & S_{3C2C} & S_{3C3C} \end{array}\right] \tag{2.6}$$

2.3.3 LO suppression

In the design of the DBC, differential excitation in port 1, should ideally provide differential signals to port 2 and 3, equally divided in amplitude and phase shifted 90° from each other. Due to asymmetries in the DBC, transformation from DM to CM occurs in S_{2C1D} and $S_{3C1D} \neq 0$. That reduces the LO to

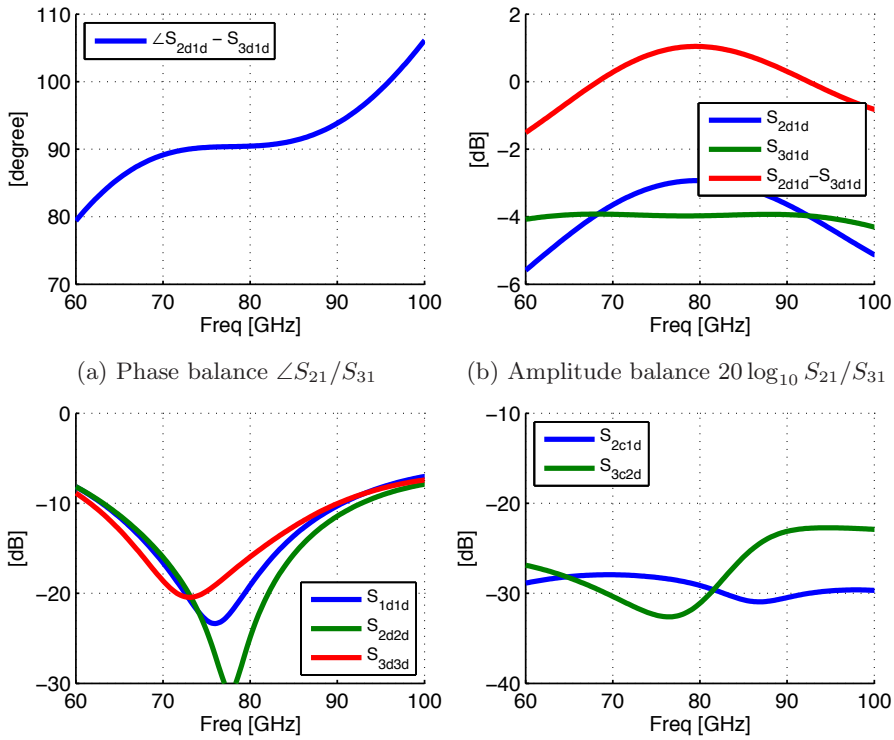

(a) Phase balance $\angle S_{21}/S_{31}$

(b) Amplitude balance $20\log_{10} S_{21}/S_{31}$

(c) Return loss

(d) CM generation

Figure 2.12: Simulated differential performance of the DBC.

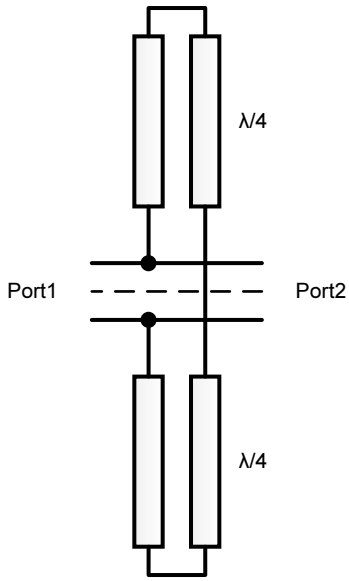

(a) Schematic

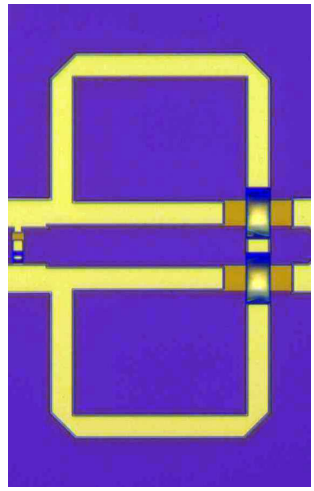

(b) Layout

Figure 2.13: Schematic and layout of the CM filter.

RF isolation of the circuit. The DM to CM generation is shown in Figure 2.12d and is approximately -25 dB. To improve the isolation, a CM filter was designed and implemented in the design. The filter is very simple but helps to reject the CM effectively. Across the differential transmission line, a $\lambda/2$ long microstrip line is connected to each of the differential lines' ends as shown in Figure 2.13a. Along the symmetry line, the electrical conditions are just the opposite for the two modes. For the CM, this symmetry line acts like a perfect magnetic boundary (an open circuit) and on the contrary for the DM, a perfect electric boundary (a short circuit). The effect is, for the CM, that the open circuit is transformed to a short circuit via the $\lambda/4$ long microstrip line. Vice versa for the DM, the virtual ground is transformed to an open circuit via the $\lambda/4$ long microstrip line. The schematic and layout of the CM filter are shown in Figure 2.13. The simulated return loss and transmission for the DM (blue) and CM (red) are shown in Figure 2.14. While maintaining good matching and low loss for the DM, the CM is effectively rejected. The ideal 4-port response of the CM filter and its mixed-mode matrix form is shown in equation 2.8. Transmission is 1 and reflection 0 for the DM and the opposite response for the CM, 0 transmission and out of phase reflection. Due to symmetry, no transformation between modes are present in this structure.

$$S_{DD} = \begin{bmatrix} S_{1D1D} & S_{1D2D} & S_{1D3D} \\ S_{2D1D} & S_{2D2D} & S_{2D3D} \\ S_{3D1D} & S_{3D2D} & S_{3D3D} \end{bmatrix} = \begin{bmatrix} 0 & \frac{-1}{\sqrt{2}} & \frac{-j}{\sqrt{2}} \\ \frac{-1}{\sqrt{2}} & 0 & 0 \\ \frac{-j}{\sqrt{2}} & 0 & 0 \end{bmatrix} \tag{2.7}$$

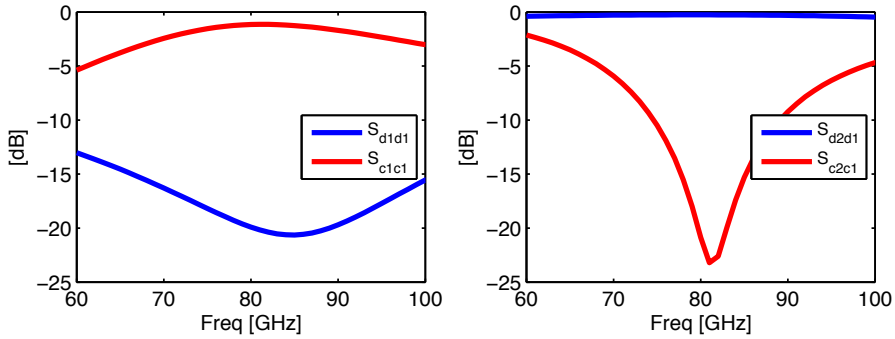

(a) Return loss (b) Transmission

Figure 2.14: Simulation results of the CM filter.

$$S = \begin{bmatrix} S_{DD} & S_{DC} \\ S_{CD} & S_{CC} \end{bmatrix} = \left[\begin{array}{cc|cc} S_{1D1D} & S_{1D2D} & S_{1D1C} & S_{1D2C} \\ S_{2D1D} & S_{2D2D} & S_{2D1C} & S_{2D2C} \\ \hline S_{1C1D} & S_{1C2D} & S_{1C1C} & S_{1C2C} \\ S_{2C1D} & S_{2C2D} & S_{2C1C} & S_{2C2C} \end{array}\right] = \left[\begin{array}{cc|cc} 0 & 1 & 0 & 0 \\ 1 & 0 & 0 & 0 \\ \hline 0 & 0 & -1 & 0 \\ 0 & 0 & 0 & -1 \end{array}\right] \tag{2.8}$$

2.3.4 Measurement setup and uncertainties

A two-tone setup was used to characterize the circuit's RF performance "on wafer" as an up-converter mixer with sweeps both in frequency and power domain. In this section the measurement setup is briefly mentioned and any uncertainties that might lead to error-nous results are discussed.

The measurements have been carried out "on wafer" using Ground-Signal-Ground (GSG)-probes for the LO and RF ports and GSGSG for the IQ ports. For the signal generation of IQ and $\overline{\text{IQ}}$, Agilent's PSG series signal synthesizers 8247C and 8257C were used in combination with external 90° and 180° degree hybrids. An HP 83650A frequency synthesizer together with mm-wave modules HP 83558A and 83557A for V- and W-band respectively were used to produce the LO signal. Finally, an HP 8565EC spectrum analyzer with Harmonic Mixers (HM) HP 11974V and 11970W was used in the setup to measure the frequency components at the RF port.

The most challenging and difficult calibration was to calibrate the HM together with the spectrum analyzer. In order to measure the IM products of the DUT, the IIP3 of the HM must be greater than the OIP3 of the Device Under Test (DUT). For this reason, an attenuator was put before the HM, large enough to measure the IM products generated from the DUT rather than the HM while still having the sensitivity to measure the low power IM products.

The phase and amplitude error from the external Intermediate Frequency (IF) hybrids contributes to the measurement inaccuracy of the circuit's balance. The hybrids from ET industries specify the balance of the 180° degree hybrid "J-112-180" to ±10° degrees and ± 0.4 dB over a frequency range 1.0-

12.4 GHz and the 90° degree hybrid "Q-112-90" to ±6° degrees and ± 0.4 dB over a frequency range 1.0-12.4 GHz. The largest inaccuracy from the measurement results are related to the external hybrids and the IRR. 20 dB IRR translates to a maximum phase imbalance of 11.5 ° degrees or a maximum amplitude imbalance of 1.75 dB. For this reason, due to the large uncertainty of the phase error of the hybrids, the accuracy of IRR is limited.

2.3.5 Results

The measurements were carried out with Continuous Waveform (CW) signals as described in section 2.3.4. The results from the measurements are summarized in Figure 2.15.

Figure 2.15a shows how the converted signal and the third and fifth IM products vary versus IF power. The extrapolated OIP3 occurs at a maximum of 13 dBm with an LO input power level of 13 dBm. Even at input IF power levels of 0 dBm, the IM suppression is more than 40 dBc.

While sweeping the LO power in Figure 2.15d and 2.15c, the response from OIP3, CL, IRR and LO-RF separation is shown. OIP3 shows a linear behavior with respect to the LO power in the range from 2 dBm to 13 dBm, where it also peaks at maximum 13 dBm. CL and IRR also improves with increased LO power, which is expected. The IRR is improved because the amplitude variation in the DBC becomes less important, due to the CL saturation. In summary, everything except RF-LO separation is benefited from a high LO drive.

In Figure 2.15b and 2.15e the LO frequency has been swept for seeing the LO bandwidth response. The CL is smooth around 11 dB and the IRR measures more than 20 dB over the E1-E3 frequency range. Taking into account the error contributions from the IF hybrids, the IRR on the circuit is most probably better than the measurement shows. Also the LO-RF isolation in Figure 2.15e is measured higher than 30 dB over all three E-bands.

In Figure 2.15f, the LO is fixed in the center of the three E-band frequency windows while sweeping the IF from -2 to 2 GHz. When the IF is negative, the side-band is measured on the Upper Side Band (USB) and RF on the Lower Side Band (LSB). When positive, the side-band is measured on the LSB side and RF on the USB, therefore the RF and sideband are on top of each other. This tell, that the high IRR and CL remain over large IF bandwidths in all three E-bands.

The results are overall very satisfying for a new concept topology which takes advantage of the CM and DM properties and make the design more compact. High linearity, high IRR and compactness over wide bandwidth make this circuit very suitable for communications in the E1, E2 and E3 frequency bands.

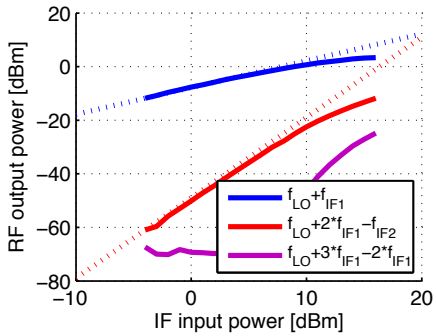

(a) 3^{rd} and 5^{th} order IM products vs P_{IF}

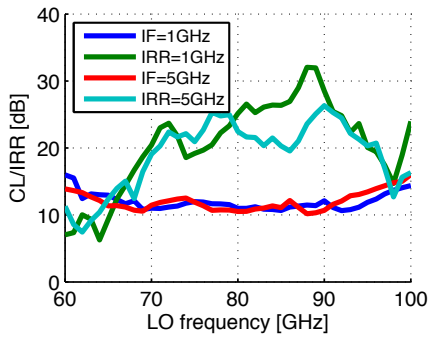

(b) CL vs f_{LO}, f_{IF} fixed at 1 GHz

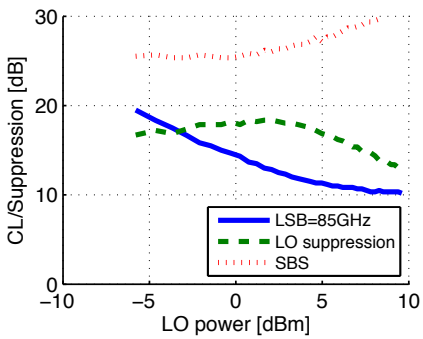

(c) CL vs P_{LO}

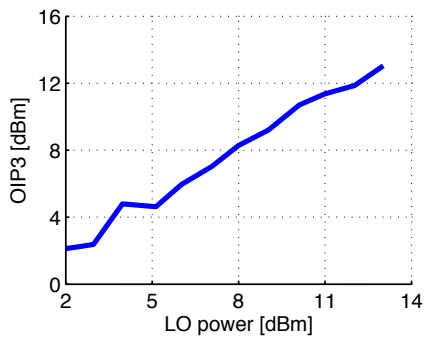

(d) OIP3 vs P_{LO}

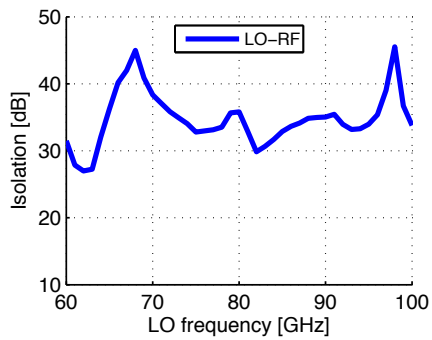

(e) LO to RF isolation

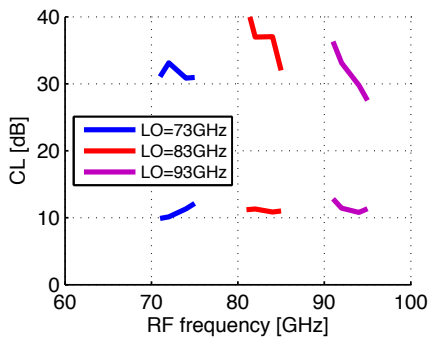

(f) CL vs f_{IF}

Figure 2.15: Summarized measurements results

2.4 Image Reject Mixer

The IRM presented in [A] is an example of a classic resistive IRM. The choice for designing a quadrature mixer comes from the expectations of using QAM modulated signals for P2P communication in the E-band. In section 2.3, the design of an up-converting IQ mixer was presented, and in this section the design and design-considerations of a down-conversion mixer is presented. In a receiver mixer, the requirements are similar to a transmitter mixer, with the difference that NF is more important and the LO-RF isolation is no longer a strong requirement. Without the need of a balanced structure, the circuit can be designed smaller and use more effectively lower LO power. The quadrature E-band mixer was reported in [A].

2.4.1 Design

In a communication receiver, linearity and NF are the two most important FOM to consider for high dynamic range. The comparison made in section 2.2.3 concludes that HEMT technology provides lower NF due to the absence of shot-noise and that the Gilbert cell is difficult to implement in a low level integration process. In terms of noise, the Schottky diode based design [22] achieves the lowest NF in the comparison, but requires high LO power which usually is the drawback of diode based mixers. For these combined reasons, the resistive mixer topology is again chosen as the basis topology.

The design of this down-converting quadrature mixer for E-band communications consists of two mixer cells, a 90° degree phase shifter, IF filters and a power combiner. Layout and schematic of the circuit are shown in Figure 2.16 and 2.17 respectively. In comparison to the single balanced mixer presented in section 2.3, this mixer provides quadrature signals but lacks features such as a balanced topology to isolate the LO and RF ports from each other. In a receiver, the reverse isolation (S_{12}) of the LNA effectively isolates the LO signal from the RF port, therefore it's usually unnecessary to add this function to the mixer. The main advantage with reduced requirements is a simpler design, more compact and requires lower LO power. The total chip size measures $2.0 \times 1.5\,\mathrm{mm}^2$, which is $0.75\,\mathrm{mm}^2$ smaller than the single balanced mixer.

To provide quadrature signals, this design uses a Lange coupler [31] for the 90° degree phase shift instead of the branchline coupler. One of the attractions with the Lange coupler is its wide bandwidth and compact layout. In Figure 2.18, the simulated amplitude and phase balance of the Lange coupler is ±2° degree and ±1 dB. In comparison to the simulated phase balance of the DBC in Figure 2.12, the response is ±2° degree to ±10° degree over the same frequency range, a considerably larger bandwidth. The amplitude balance is ±2 dB and ±1 dB in favor to the DBC. The Lange coupler is fed to the gates of the mixer for more reasons than providing quadrature signals. First, the gates of FETs are in general difficult to match to 50 Ω over a wide bandwidth due to the capacitive input network and high transformation ratio. Therefore, the Lange coupler on the LO will provide excellent match to this otherwise difficult port to match. Second, amplitude imbalance of the Lange coupler is less important due to CL saturation with LO power. Figure 2.20c illustrates how the CL saturates with LO power, therefore the IQ amplitude balance can

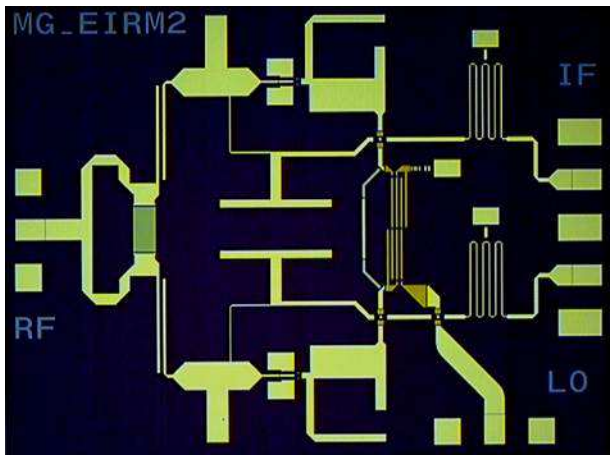

Figure 2.16: Layout

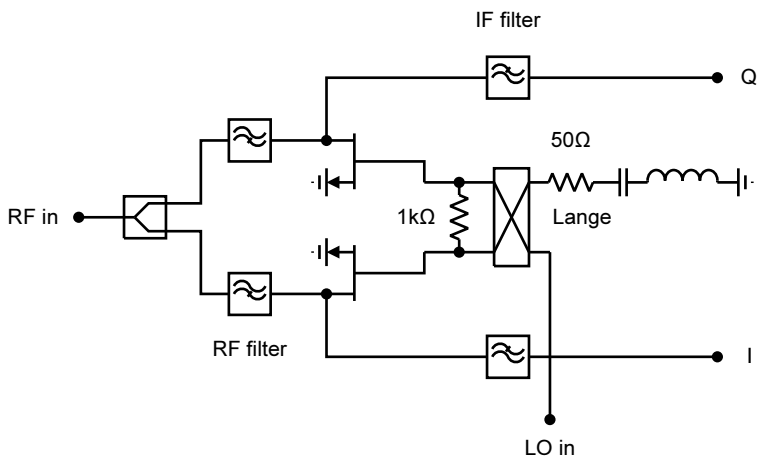

Figure 2.17: Schematic

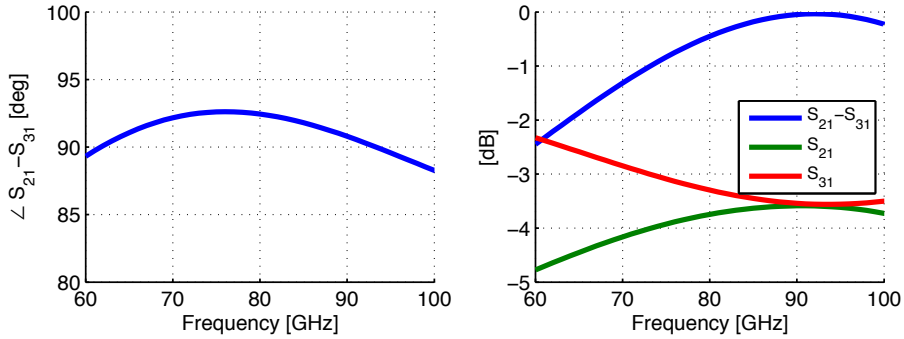

(a) Phase balance (b) Amplitude balance

Figure 2.18: Simulated amplitude and phase balance of the Lange coupler

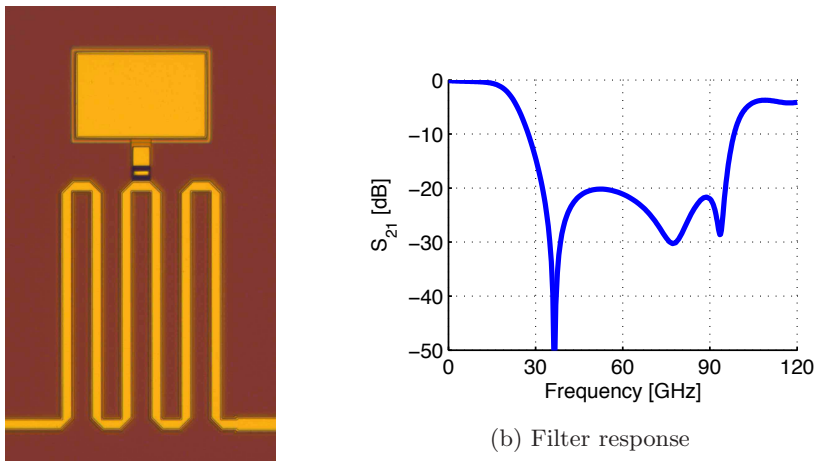

(a) Filter layout (b) Filter response

Figure 2.19: Layout and simulated transmission response of the IF filter

be better than that of the Lange coupler.

Filter bandwidth is of key importance to send high speed, large bandwidth data. Therefore it's critical to design on chip filtering properly to cover the frequency range of the RF. A compact low pass filter is implemented with modifications from the original idea in order to make it more compact [32]. The lines are folded and the open stub is changed to a capacitor to ground. The filter layout is shown in Figure 2.19a and its electrical response in Figure 2.19b respectively. Off chip, components with higher capacitance and inductance with lower self resonance frequency can be used to limit the bandwidth and noise further.

2.4.2 Results

The measurements were carried out "on wafer" with CW signals to analyze its RF performance. The results from the verification of the circuit is sum-

marized in Figure 2.20. In Figure 2.20a, the CL and IRR are plotted versus LO frequency, with the IF frequency fixed at 1 GHz. CL is average to good for a resistive mixer, between 7-10 dB in the E-band which is the lowest reported CL for an E-band resistive mixer. IRR is measured higher than 13 dB and peaks close to 40 dB at 78 GHz. Considering the simulation results of the Lange coupler in Figure 2.18, IRR would expect to be higher, especially in the upper part of the E-band. On the lower side of the band, the amplitude imbalance is higher and this could in fact be a reason for the lower IRR. With higher LO power this can be improved as was described in section 2.4.1. At the upper part of the E-band, the reason for the lower IRR is more difficult to determine. Both the amplitude and phase balance look the best for the Lange coupler. The Lange coupler simulations are though performed in a 50 Ω environment, something which is not guaranteed in the circuit design. Figure 2.20c shows the CL vs LO power for a fixed LO and IF frequency of 80 GHz and 1 GHz respectively. Figure 2.20d shows the CL versus RF power with the same conditions as the LO power sweep. The Input referred P1dB (IP1dB) occurs at 0 dBm, which is lower than for the single balanced IQ mixer in [B], but still considered good for a receiver mixer. The high IRR, low CL and high linearity makes this IRM a good choice for communications in the E-band.

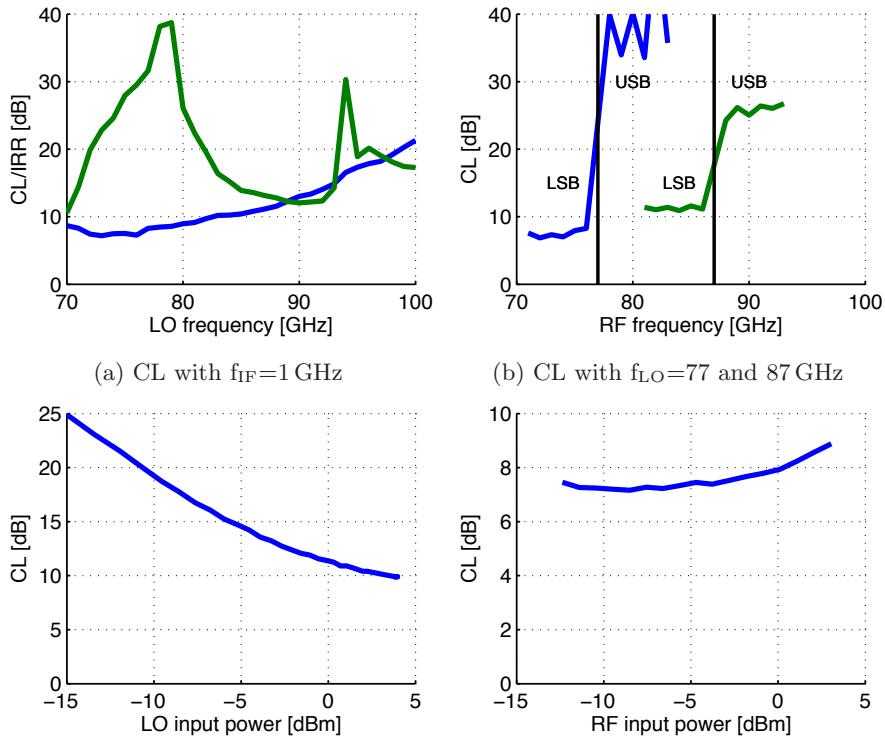

(a) CL with f_{IF}=1 GHz

(b) CL with f_{LO}=77 and 87 GHz

(c) CL versus P_{LO}

(d) CL versus P_{RF}

Figure 2.20: Measurement results of the quadrature down-converting mixer

Chapter 3

53 GHz single chip receiver

Weather conditions have always been of interest to the human being. In the nordic countries the prediction and accuracy of the weather forecasts has always been a subject of discussion. Apart from the common interest from the public, many businesses rely on accurate weather services and are willing to pay for more predictable now casting services. Long term climate effects are generally not covered from this application.

Meteorologists now look for alternative solutions to achieve more accurate short term weather predictions. Future mm and sub-mm radiometers for remote sensing in GEO are studied and compared with Low Earth Orbit (LEO) [33]. The primary advantage with GEO is its continuous coverage of a large area of the earth's atmosphere. Moreover, temperature and humidity profiles with high horizontal resolution under all weather conditions make this solution very attractive for nowcasting service. Especially interesting are frequencies close to the water vapour and oxygen absorption lines at 60, 118, 183 and 380 GHz. In Figure 3.1, the attenuation levels for oxygen and water vapour are separatly plotted from the overall atmosphere attenuation with clear resonances at the mentioned frequency points. With the advances made in semiconductor technologies it's possible to make such radiometer systems for mm-wave and sub-mm wave with MMIC solutions.

In 2007, a Geostationary Atmospheric Sounder (GAS) demonstrator was built with 20 elements of 53 GHz receiver chips. When built, the complete GAS will consist of 136 elements of 53 GHz receivers, 107 elements of 118, 183 and 380 GHz with a total power consumption and mass budget of 300 W and 300 kg respectively [6]. For the demonstrator, a 53 GHz single chip MMIC was developed from Chalmers [34], but power consumption and IQ balance especially needed to be improved to fulfill the requirements. For this reason, this second generation single chip 53 GHz receiver chip with a new LNA, $\times 4$ frequency multiplier and IRM was designed to improve power consumption, IRR and NF.

3.1 Design

The receiver chip consists of a $\times 4$ frequency multiplier, an IQ mixer and an LNA integrated on the chip. Integration of mixed functions into a single chip

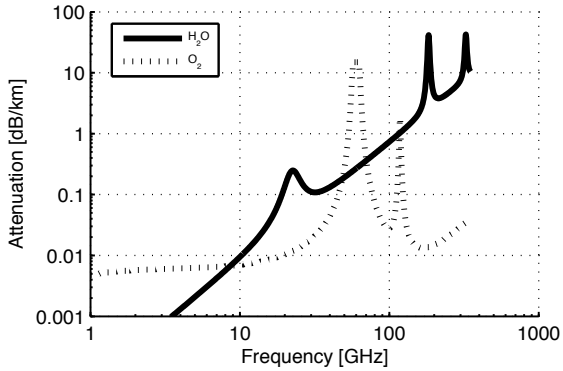

Figure 3.1: Absorption lines for oxygen and water vapour

has been reported in [35] and claim increased yield and improved RF performance. Apart from the fact that solder and wire bonding several individual MMIC circuits to create a receiver chipset is time consuming, it also makes yield poorer due to inaccuracy of wire bonds. Below follows a description of the complete receiver and its sub-blocks.

Single chip receiver

The layout and block diagram of the 53 GHz single chip receiver are shown in Figures 3.2a and 3.2b respectively. On the lower left part of the circuit, the $\times 4$ frequency multiplier is located. To the upper left is located, a three stage LNA providing good gain, matching and NF to the overall receiver. Finally, a IRM very similar to that designed in chapter 2, section 2.4 is located to the upper right of the circuit.

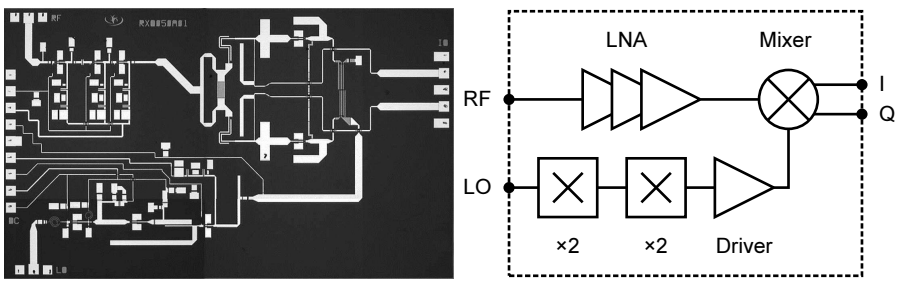

(a) Layout (b) Schematic

Figure 3.2: Layout and schematic of this 53 GHz receiver chip

LNA

The LNA in the single chip receiver was redesigned to improve both the power consumption and NF. The changes to improve the numbers were to remove the negative resistive feed-back to a common-source design and resize the transistors from $2 \times 50\ \mu m$ to $2 \times 25\ \mu m$ on the first two stages. This should, for the same V_{gs} lower the power consumption with

1/3. The schematic of the LNA is shown in Figure 3.3 and a close-up of the layout in Figure 3.4. The design is more compact than before and measures NF as low as 3.5 dB with good gain and matching. The return loss and gain from the breakout circuit are shown in figure 3.5b.

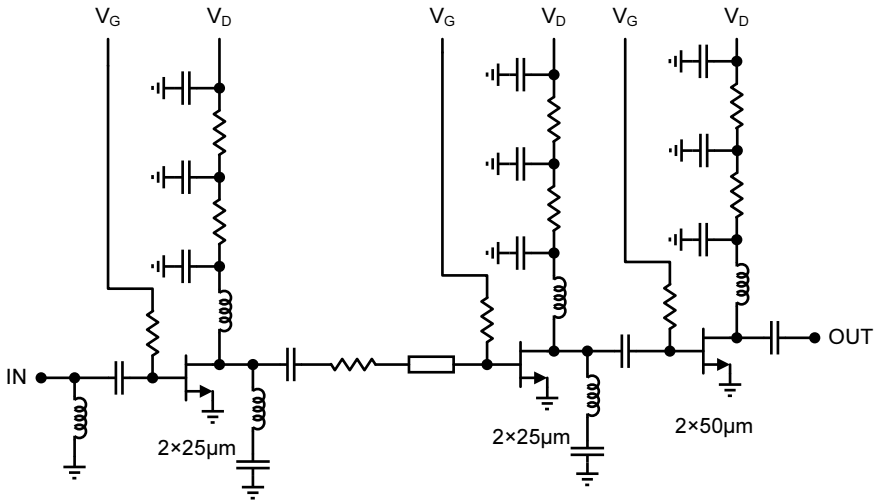

Figure 3.3: Schematic of the LNA

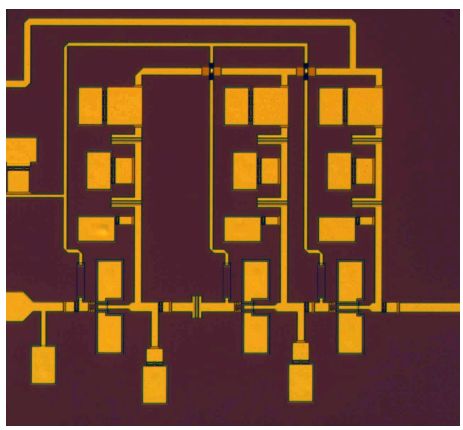

Figure 3.4: Layout of the LNA

IRM

The mixer is a scaled version of that presented in chapter 2, section 2.4. The reader is referred to section 2.4 for understanding of the design.

×4 frequency multiplier

The ×4 frequency multiplier consists of two cascaded doublers followed by a buffer amplifier to boost the output power to the mixer. The two

×2 transistors, biased in class B are the same size as be before; 2 × 50 μm but the driver stage is changed to a smaller sized transistor. Again, to reduce the power consumption but still deliver enough gain and output power. The active common-gate input matching stage on the multiplier is removed and changed to a passive network to reduce the power consumption. The results from the breakout circuit are shown in figure 3.5a, showing the first five harmonics with the fourth harmonic highlighted.

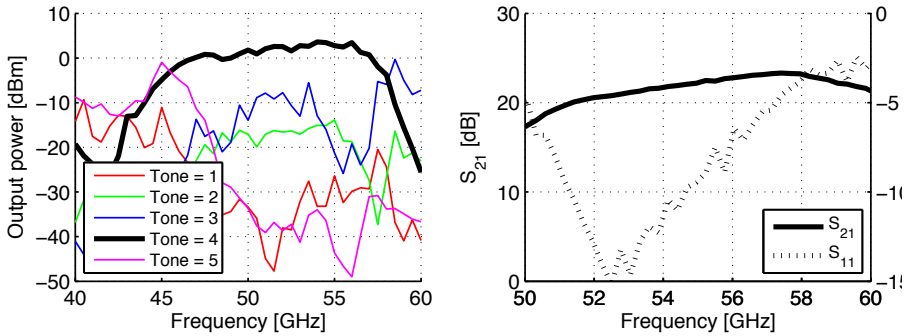

(a) Measured harmonics from the multiplier.

(b) S-parameter measurement on the LNA in the receiver band. Shown are S_{11} and S_{21}

Figure 3.5: Measurements from breakouts of the receiver chip.

3.2 Results and comparison

The circuit characterization was made "on wafer", measuring S-parameters, IM products and NF.

Figure 3.6a shows the CG and IRR of the whole receiver. LO frequency is fixed at 49 GHz (the 4^{th} harmonic) and the RF frequency is swept from 50 to 58 GHz to measure the CG. For the IRR, the RF is swept on both sides of the fixed LO, reading very high numbers of IRR due to the combination of the IRM and the frequency selective LNA. At 50 GHz the IRR is better than 47 dB, an improvement with 34 dB.

NF is of utmost importance to be able to detect the most weak signals. In contrast to communication links, focus is to detect the weakest signal levels instead of a high dynamic range, therefore linearity is not a concern. In Figure 3.6b, the measured NF of the receiver is shown and in comparison to published work at 53 GHz, this measures the lowest. The transistion at 54 GHz, where the NF increases with 1 dB for no obvious reason, all sub-blocks show smooth response in this frequency range. In Figure 3.6c, the linearity has been evaluated with 2-tone, showing both second and third IM products with the input power level being swept from -40 to -30 dBm. The extrapolation of the IM products show the IP2 and IP3 levels.

Table 3.1 summarizes the results of receivers in this frequency range. The lowest NF for a 53 GHz receiver is reported in this circuit, 1.4 dB lower NF at

room temperature than any of the receivers in the comparison, a big difference and improvement over [34]. IRR is also by far better than the reported numbers in [34] [35], better than $> 47\,\mathrm{dB}$ in comparison to $13\,\mathrm{dB}$. The smallest size, highest gain and lowest power consumption are however all exhibited in CMOS circuits [36] [37], but the NF is not the best, as expected.

Ref	Freq [GHz]	p_{LO}	CG	NF	IRR	IF BW	P_{DC}	IIP3	Size [mm^2]	Process
[34]	49-54	0	13	6.3	13	0-5	360	-11	14.1	0.15 μm mHEMT
[36]	49-53	-	26	8.3	-	-	80	-25.5 (IP1dB)	0.15	90 nm CMOS
[37]	51-54	-	21	6	-	4-5.5	60	-21 (IP1dB)	0.3	90 nm CMOS
[35]	54.5-64.5	-2	13	7.2	13	1.3-3.2	450	-10	22	0.15 μm pHEMT
paper C	50-60	5	10	4.6	$>$ 47	0-10	140	-12	11.3	0.15 μm mHEMT

Table 3.1: Comparison of 53 GHz receivers

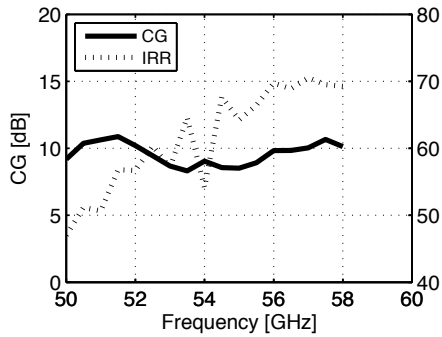

(a) CG and IRR

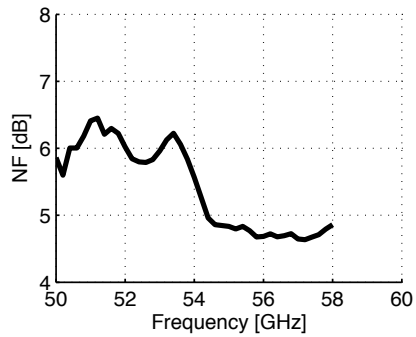

(b) NF

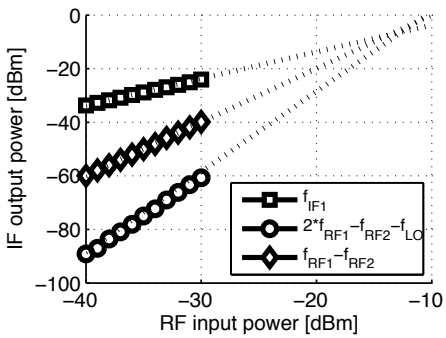

(c) Second and third order IM products measured on the receiver

Figure 3.6: Measured FOM on the receiver.

Chapter 4

Conclusions

Two resistive quadrature MMIC mixers have been designed in a 0.15 μm mHEMT technology for wideband communications at E-band, most commonly referred to 71-76 and 81-86 GHz. The two mixers show excellent performance over wide RF and IF bandwidths and state-of-the-art OIP3 for a resistive mixer. A novel differential branchline coupler was used in the design in paper B to add LO-RF isolation to the circuit while minimizing size and adding functionality. The increase in size was only 25% in comparison to the circuit in paper A, a similar circuit without this function. In addition to added functionality, the properties of DM and CM signals were shown to be beneficial for further improving the balance. DM signals are often used in CMOS and BiCMOS due to the lossy substrate but they are not commonly used in GaAs HEMT. The results and implementation of the design in paper B with differential signals showed improved performance and small size. The broadband, smooth CL, high IRR and high linearity makes both IQ modulators very well suited for E-band RF-frontends.

A 53 GHz single chip receiver for atmospheric remote sensing in GEO was designed, fabricated and characterized. Its performance show state-of-the-art NF, 1.4 dB lower than any published 53 GHz receiver. The power saving design, low NF and high IRR make this single chip receiver suited for atmospheric remote sensing.

4.1 Future work

Wideband communication in the mm- and sub-mm wave (220 and 340 GHz) are interesting frequency windows for high data rate communication due to their vast available bandwidths and relatively low atmospheric attenuation. The high carrier frequency makes the relative RF bandwidth smaller to effectively support larger data bandwidths. Data bandwidths up to or beyond 30 GHz can possibly reach 100 Gbps with fairly simple modulation. Emerging technologies, such as SiGe and InP HBT support medium-, large- and very large scale integration levels with high f_T/f_{max} to allow complete integration with RF front-ends together with back-end digital circuits to be designed on a single chip. Integration of more circuit blocks on chip, especially baseband circuits are intriguing ideas to try for increasing wireless transmission data rates.

Acknowledgment

I cannot conclude this work without thanking the people that made this possible.

A very special thank you I want to express to my examiner and supervisor Prof. Herbert Zirath. He welcomed me to Microwave Electronics Laboratory (MEL) already in 2004 to do my master's thesis. Later, in 2007 he gave me the opportunity to come back to Chalmers to participate in a project for market related research on high frequency circuit design together with the possibility of starting a company based on the research carried out at MEL. In 2009 came the opportunity to combine this work with the research at MEL in order to pursue a Ph.D., a possibility I'm very grateful for. His expertise of circuit design and cross disciplinary knowledge has been the base and inspiration of this work.

I wish to thank my co-supervisor Sten Gunnarsson for taking part in my work with discussions and guidance. He introduced me to the field of microwave circuits, an area I enjoy very much working with.

I would like to thank my co-supervisor Mattias Ferndahl for all the technical discussions and unconditional assistance in the lab.

A special thanks goes to Trajan Badju for supporting the research work being pursued at MEL and for being an excellent boss and friend.

A thank you is also directed to Iltcho Angelov for broadening the context of this work and his enthusiasm to teach me about device modeling and other related topics.

I want to acknowledge Bertil Hansson for making, always with enthusiasm, great design-kits to work with.

I also want to thank my colleagues and friends; Zhongxia (Simon), Oliver, Olle, Cesar, Morteza and all the people at MEL and Gotmic for making them great places to work at.

I express my deepest gratitude to Helena, my family and friends for all the support and love I get from them.

Finally, I would like to acknowledge the financing institutions and collaboration partners which made this work possible. This work has been supported by "Vinn Verifiering" which is funded by Swedish Governmental Agency of Innovation Systems (VINNOVA) and "System on chip solutions for future high speed communication" which is funded by Swedish Foundation for Strategic Reasearch (SSF). Gotmic for supporting and funding tapeouts and publishing academic material. WIN semiconductors is acknowledged for processing the circuits.

Bibliography

[1] W. R. Deal, K. Leong, V. Radisic, S. Sarkozy, B. Gorospe, J. Lee, P. H. Liu, W. Yoshida, J. Zhou, M. Lange, R. Lai, and X. B. Mei, "Low Noise Amplification at 0.67 THz Using 30 nm InP HEMTs," *Microwave and Wireless Components Letters, IEEE*, vol. 21, no. 7, pp. 368–370, 2011.

[2] A. Fehske, G. Fettweis, J. Malmodin, and G. Biczok, "The global footprint of mobile communications: The ecological and economic perspective," *Communications Magazine, IEEE*, vol. 49, no. 8, pp. 55–62, 2011.

[3] "Cisco Visual Networking Index (VNI): Global Mobile Data Traffic Forecast Update, 2012-2017," 2012.

[4] "Radio-frequency arrangements for fixed service systems," 2012-03 2012.

[5] J. Wells, "Faster than fiber: The future of multi-G/s wireless," *Microwave Magazine, IEEE*, vol. 10, no. 3, pp. 104–112, 2009.

[6] J. Christensen, A. Carlstrom, H. Ekstrom, A. Emrich, J. Embretsen, P. De Maagt, and A. Colliander, "GAS: the Geostationary Atmospheric Sounder," in *Geoscience and Remote Sensing Symposium, 2007. IGARSS 2007. IEEE International*, pp. 223–226.

[7] M. Willis, "Propagation tutorial," 2007. [Online]. Available: http://www.mike-willis.com/Tutorial/PF5.htm

[8] S. Voinigescu, *High-Frequency Integrated Circuits*. The Cambridge RF and Microwave Engineering Series, 2013.

[9] C. Jingjing, H. Zhongxia, B. Lei, C. Svensson, L. Yinggang, S. Gunnarsson, C. Stoij, and H. Zirath, "10 Gbps 16QAM transmission over a 70/80 GHz (E-band) radio test-bed," in *Microwave Integrated Circuits Conference (EuMIC), 2012 7th European*, pp. 556–559.

[10] A. Hirata, T. Kosugi, H. Takahashi, R. Yamaguchi, F. Nakajima, T. Furuta, H. Ito, H. Sugahara, Y. Sato, and T. Nagatsuma, "120-GHz-band millimeter-wave photonic wireless link for 10-Gb/s data transmission," *Microwave Theory and Techniques, IEEE Transactions on*, vol. 54, no. 5, pp. 1937–1944, 2006.

[11] J. Antes, D. Lopez-Diaz, U. J. Lewark, S. Wagner, A. Tessmann, A. Leuther, and I. Kallfass, "A high linearity I/Q mixer for high data rate E-band wireless communication links," in *Microwave Integrated Circuits Conference (EuMIC), 2012 7th European*, pp. 278–281.

[12] B. Gilbert, "A precise four-quadrant multiplier with subnanosecond response," *Solid-State Circuits, IEEE Journal of*, vol. 3, no. 4, pp. 365–373, 1968.

[13] L. A. NacEachern and T. Manku, "A charge-injection method for Gilbert cell biasing," in *Electrical and Computer Engineering, 1998. IEEE Canadian Conference on*, vol. 1, pp. 365–368 vol.1.

[14] O. Mitrea, C. Popa, A. M. Manolescu, and M. Glesner, "A linearization technique for radio frequency CMOS Gilbert-type mixers," in *Electronics, Circuits and Systems, 2003. ICECS 2003. Proceedings of the 2003 10th IEEE International Conference on*, vol. 3, pp. 1086–1089 Vol.3.

[15] B. Gilbert, "The MICROMIXER: a highly linear variant of the Gilbert mixer using a bisymmetric Class-AB input stage," *Solid-State Circuits, IEEE Journal of*, vol. 32, no. 9, pp. 1412–1423, 1997.

[16] W. Li, R. Kraemer, and J. Borngraeber, "An Improved Highly-Linear Low-Power Down-Conversion Micromixer for 77 GHz Automotive Radar in SiGe Technology," in *Microwave Symposium Digest, 2006. IEEE MTT-S International*, pp. 1834–1837.

[17] S. A. Maas, "A GaAs MESFET Mixer with Very Low Intermodulation," *Microwave Theory and Techniques, IEEE Transactions on*, vol. 35, no. 4, pp. 425–429, 1987.

[18] S. A. Maas, *Microwave Mixers, Second Edition.* Norwood, MA: Artech House, 1992.

[19] M. Varonen, M. Karkkainen, J. Riska, P. Kangaslahti, and K. A. I. Halonen, "Resistive HEMT mixers for 60-GHz broad-band telecommunication," *Microwave Theory and Techniques, IEEE Transactions on*, vol. 53, no. 4, pp. 1322–1330, 2005.

[20] K. Sung-Chan, A. Dan, L. Byeong-Ok, T. J. Baek, S. Dong-Hoon, and R. Jin-Koo, "High-performance 94-GHz single balanced mixer using 70-nm MHEMTs and surface micromachined technology," *Electron Device Letters, IEEE*, vol. 27, no. 1, pp. 28–30, 2006.

[21] C. Wagner, M. Hartmann, A. Stelzer, and H. Jaeger, "A Fully Differential 77-GHz Active IQ Modulator in a Silicon-Germanium Technology," *Microwave and Wireless Components Letters, IEEE*, vol. 18, no. 5, pp. 362–364, 2008.

[22] T. N. Ton, T. H. Chen, K. W. Chang, H. Wang, T. L. Tan, G. S. Dow, G. M. Hayashibara, B. Allen, and J. Berenz, "A W-band monolithic InGaAs/GaAs HEMT Schottky diode image reject mixer," in *Gallium Arsenide Integrated Circuit (GaAs IC) Symposium, 1992. Technical Digest 1992., 14th Annual IEEE*, pp. 63–66.

[23] Y. Hamada, K. Maruhashi, M. Ito, S. Kishimoto, T. Morimoto, and K. Ohata, "A 60-GHz-band Compact IQ Modulator MMIC for Ultra-high-speed Wireless Communication," in *Microwave Symposium Digest, 2006. IEEE MTT-S International*, pp. 1701–1704.

[24] C. Hong-Yeh, H. Tian-Wei, W. Huei, W. Yu-Chi, C. Pane-Chane, and C. Chung-Hsu, "Broad-band HBT BPSK and IQ modulator MMICs and millimeter-wave vector signal characterization," *Microwave Theory and Techniques, IEEE Transactions on microwave theory and techniques*, vol. 52, no. 3, pp. 908–919, 2004.

[25] T. Jeng-Han, W. Pei-Si, L. Chin-Shen, H. Tian-Wei, J. G. J. Chern, and H. Wen-Chu, "A 25-75 GHz Broadband Gilbert-Cell Mixer Using 90-nm CMOS Technology," *Microwave and Wireless Components Letters, IEEE*, vol. 17, no. 4, pp. 247–249, 2007.

[26] T. Mimura, S. Hiyamizu, T. Fujii, and K. Nanbu, "A New Field-Effect Transistor with Selectively Doped GaAs/n-$Al_xGa_{1-x}As$ Heterojunctions," *Japanese Journal of Applied Physics*, vol. 19, no. 5, pp. 225–227, 1980.

[27] M. Abbasi, T. Kjellberg, S. E. Gunnarsson, and H. Zirath, "Direct carrier quadrature modulator and Demodulator MMICs for 60 GHz gigabit wireless communications," in *Microwave Conference Proceedings (APMC), 2011 Asia-Pacific*, pp. 1134–1137.

[28] Agilent Technologies, "Circuit components: nonlinear devices," pp. 261–308, 2008.

[29] E. J. G. Matthaei, L. Young, *Microwave Filters, Impedance-Matching Networks and Coupling Structures.* Artech House, 1980.

[30] D. E. Bockelman and W. R. Eisenstadt, "Combined differential and common-mode scattering parameters: theory and simulation," *Microwave Theory and Techniques, IEEE Transactions on*, vol. 43, no. 7, pp. 1530–1539, 1995.

[31] N. Marchand, "Transmission-Line Conversion transformers," *Electronics*, vol. 17, no. December, pp. 142–145, 1944.

[32] L. Rui and K. Dong Il, "A new compact low-pass filter with broad stop-band and sharp skirt characteristics," in *Microwave Conference Proceedings, 2005. APMC 2005. Asia-Pacific Conference Proceedings*, vol. 3, p. 3 pp.

[33] U. Klein, L. Chung-Chi, N. Atkinson, J. Charlton, and C. Philpot, "Future microwave radiometers in geostationary and medium earth orbit," in *Geoscience and Remote Sensing Symposium, 2003. IGARSS '03. Proceedings. 2003 IEEE International*, vol. 3, pp. 2158–2160.

[34] S. E. Gunnarsson, A. Emrich, H. Zirath, R. Kozhuharov, C. Karnfelt, J. Embretsen, and C. Tegnander, "A single-chip 53 GHz radiometer front-end MMIC for geostationary atmospheric measurements," in *Radio and Wireless Symposium, 2008 IEEE*, pp. 867–870.

[35] S. E. Gunnarsson, C. Karnfelt, H. Zirath, R. Kozhuharov, D. Kuylenstierna, A. Alping, and C. Fager, "Highly integrated 60 GHz transmitter and receiver MMICs in a GaAs pHEMT technology," *Solid-State Circuits, IEEE Journal of*, vol. 40, no. 11, pp. 2174–2186, 2005.

[36] B. Razavi, "A Millimeter-Wave CMOS Heterodyne Receiver With On-Chip LO and Divider," *Solid-State Circuits, IEEE Journal of*, vol. 43, no. 2, pp. 477–485, 2008.

[37] D. Alldred, B. Cousins, and S. P. Voinigescu, "A 1.2V, 60-GHz radio receiver with on-chip transformers and inductors in 90-nm CMOS," in *Compound Semiconductor Integrated Circuit Symposium, 2006. CSIC 2006. IEEE*, pp. 51–54.

Paper A

An Image Reject Mixer for High-Speed E-band (71-76, 81-86 GHz) Wireless Communication

Marcus Gavell, Mattias Ferndahl, Sten E. Gunnarsson, Morteza Abbasi, Herbert Zirath

Paper B

A linear 70-95 GHz differential IQ modulator for E-band Wireless Communication

Marcus Gavell, Herbert Zirath, Mattias Ferndahl, Sten E. Gunnarsson

Paper C

A 53 GHz single chip Receiver for Geostationary Atmospheric Measurements

Marcus Gavell, Mattias Ferndahl, Sten E. Gunnarsson, Herbert Zirath